Mechanism and Kinetics of Fentanyl Dissociation from the μ-Opioid Receptor

Paween Mahinthichaichan,[†,‡] Quynh Vo,[†,‡] Christopher R. Ellis,[¶] and Jana Shen[*,‡]

† *Center for Drug Evaluation and Research, United States Food and Drug Administration, Silver Spring, MD 20993, United States*

‡ *Department of Pharmaceutical Sciences, University of Maryland School of Pharmacy, Baltimore, MD 21201, United States*

¶ *United States Army, DEVCOM Chemical Biological Center, Aberdeen Proving Ground, MD 21010, United States*

Received April 25, 2021; E-mail: jana.shen@rx.umaryland.edu

Abstract: Fentanyl is a main driver of the current opioid crisis. As a powerful narcotic, fentanyl initiates biological response through binding to the μ-opioid receptor (mOR); however, the molecular details remain unknown. Here we study the mechanism and predict the kinetics of fentanyl-mOR dissociation by applying an advanced molecular dynamics (MD) technique based on the X-ray structure of the morphinan bound mOR. 144 metadynamics trajectories were performed while accounting for the protonation state of the conserved H297$^{6.52}$, which has been suggested to modulate ligand-mOR affinity and binding mode. Surprisingly, in some trajectories fentanyl samples a deep pocket 5–10 Å below the level of the conserved D147$^{3.32}$ before escaping mOR, yielding the calculated residence times of 27 s, 6 s, and 0.6 s, in the presence of the ND-, NE-, and doubly protonated H297$^{6.52}$, respectively. The former value is within one order of magnitude from the recently measured residence time of $\sim$4 min, suggesting the biological relevance of fentanyl's deep insertion, which is enabled through hydrogen bonding with H297$^{6.52}$ as well as hydrophobic interactions with transmembrane helix 6. These data support the hypothesis that the molecular mechanism of fentanyl may be distinct from morphinan compounds. Our developed protocol may be used to predict the dissociation rates of other opioids, thereby assisting the evaluation of strategies for drug overdose reversal. Finally, the profound role of the histidine protonation state discovered in this work may shift the paradigm in computational studies of ligand-receptor kinetics.

INTRODUCTION

Opioids are powerful painkillers but also among the most abused drugs.[1,2] In 2017, the US Department of Health and Human Services declared the opioid crisis a public health emergency. According to data from the Centers for Disease Control and Prevention,[3] a record number of 81,000 drug overdose deaths occurred in 2019-2020 and the main driver of the increase is synthetic opioids, primarily illicitly manufactured fentanyl, which is often pressed into counterfeit pills or mixed with heroin or cocaine. Fentanyl is a controlled prescription narcotic and depending on the route of administration 10-400 times more potent than morphine.[4] The significant rise in overdose deaths from illicitly produced nonpharmaceutical fentanyl has been attributed to fentanyl's high potency, fast onset, and low manufacturing cost.[4,5] Additionally, the ease of structural modifications has led to the emergence of illicit fentanyl analogs,[5] which may have even higher potency and abuse potential.

The main molecular target of fentanyl is the μ-opioid receptor (mOR),[6] a class A G-protein coupled receptor (GPCR) comprised of seven transmembrane (TM) helices (Fig. 1a-c). Fentanyl binds to mOR, inducing conformational changes which enable the receptor to associate with G-protein and β-arrestin and activate the related signaling pathways. Current treatment of opioid overdose relies on the use of naloxone, an antagonist that binds to mOR and deactivates the signaling. Mechanistically, naloxone works by preventing the dissociated opioid from rebinding. Thus, understanding the fentanyl-mOR unbinding mechanism and kinetics is relevant for evaluating strategies used for overdose reversal.

An experimental structure of mOR bound to fentanyl or fentanyl-like opioid is lacking; however, the X-ray co-crystal structures of mOR in complex with the morphinan agonist BU72[7] and antagonist β-FNA,[8] as well as the cryogenic electron microscopy (cryo-EM) model of mOR in complex with an endogenous peptide analog DAMGO[9] were recently obtained. These structures revealed an orthosteric binding site common to class A GPCRs,[10] which is located near the center of the receptor, involving transmembrane helices (TMs) 2, 3, 5, 6 and 7 (Fig. 1a-c). In this site, the ligand forms a salt bridge between the piperidine amine and D147$^{3.32}$ on TM3 (superscript refers to the Ballesteros-Weinstein numbering[11]), consistent with an earlier mutagenesis experiment demonstrating that alanine substitution of D147$^{3.32}$ reduces mOR's affinity for morphine, DAMGO, and naloxone.[12] Fentanyl also possesses a piperidine in its core (Fig. 1d), and the piperidine-D147$^{3.32}$ binding mode has been recently validated by molecular docking[13] and molecular dynamics (MD) simulations.[14–16] Nonetheless, fentanyl and morphine differ significantly in their structures and signaling biases, which has been speculated as a result of different binding and activation mechanisms.[5]

Using multiple MD techniques including the continuous constant pH and weighted-ensemble (WE) methods,[16] we recently found that fentanyl can adopt a secondary binding mode through hydrogen bonding between the piperidine and the conserved H297$^{6.52}$ on TM6. Intriguingly, the H297-binding mode only occurred in the simulations with the neutral Hid297 state.[16] The charge state of H297$^{6.52}$ has been repeatedly suggested as important for mOR's ligand recognition and activity; however, the precise role of H297$^{6.52}$ remains unclear. Mutagenesis experiments showed that at low pH whereby H297$^{6.52}$ is likely protonated, mOR's affinities for DAMGO and naloxone are reduced;[12,17] however, the mea-

surement conducted with fentanyl was inconclusive.[18]

MD simulations have been increasingly applied to the study of ligand-receptor kinetics.[19–23] In this work we use an enhanced sampling MD technique called well-tempered metadynamics[24,25] to examine fentanyl's dissociation mechanism and kinetics as well as to further probe the role of H297$^{6.52}$. In metadynamics bias potentials are deposited along chosen collective variables to overcome free energy barriers. As such metadynamics is an efficient method for exploring protein-ligand unbinding kinetics,[26–29] bridging the microsecond simulation and the second-to-minute experimental timescales. Most recently, metadynamics simulations of morphine and buprenorphine dissociation from mOR showed that the ligand transitioned to the vestibule region after the D147$^{3.32}$ salt bridge was disrupted.[23] We carried out a total of 144 metadynamics simulations with different H297$^{6.52}$ protonation states, and surprisingly, in about 28% of the trajectories fentanyl sampled positions 1–10 Å below the orthosteric site before dissociation. Remarkably, while the calculated dissociation time for the pathways whereby fentanyl escapes from the orthosteric site is in the millisecond range, it is prolonged to 0.1–10 s depending on the H297$^{6.52}$ protonation state in the trajectories involving deep insertion. The latter, particularly that with Hid297 is within one order of magnitude from the recently measured value. We explored the mechanism of fentanyl's deep insertion in mOR and the effect of the H297$^{6.52}$ protonation state. This work represents a first step towards large-scale predictive modeling of the dissociation kinetics of fentanyl analogs, which may be used to assist in the evaluation of strategies for opioid overdose treatments.

RESULTS AND DISCUSSION

Metadynamics simulations of fentanyl-mOR dissociation revealed a deep insertion mechanism. 48 independent well-tempered metadynamics[25] runs were performed with each protonation state of H297: Hid (proton on ND), Hie (proton on NE), and Hip (doubly protonated). The simulations were initiated from the equilibrated fentanyl-mOR complex structure in which fentanyl is bound in the orthosteric site stabilized by a salt-bridge between the piperidine amine and D147 (Fig. 1a-c and Fig. S1); this binding mode has been recently validated by μs MD simulations.[14–16] To drive the dissociation of fentanyl, a biasing potential was deposited every 10 ps along two collective variables, fentanyl's center of mass (COM) z position (Fig. 1) and the fentanyl-mOR contact number (See SI Eq. 1). When fentanyl is bound in the orthosteric site, its z position is 1–4 Å and contact number is 150–250, and when fentanyl is dissociated, it is near the solvent accessible entrance of the receptor, with z above 15 Å and contact number less than 100. The biased metadynamics time of dissociation ranged from 10 to 90 ns (Fig. S2). For clarity, we will omit the superscript (Ballesteros-Weinstein numbering[11]) in the following discussion. We will refer to trajectories with Hid297 Hie297, and Hip297 as Hid, Hie, and Hip trajectories, respectively.

Close examination of the trajectories revealed two types of dissociation pathways. 73% Hid, 63% Hie, and 81% Hip trajectories followed the "direct" pathways, in which fentanyl spontaneously unbinds after sampling the orthosteric site region, with concurrent increase in fentanyl's z position and decrease in the contact number. The direct pathway mechanism corroborates a recent metadynamics study of the dissociation of morphine and analog buprenorphine from mOR by

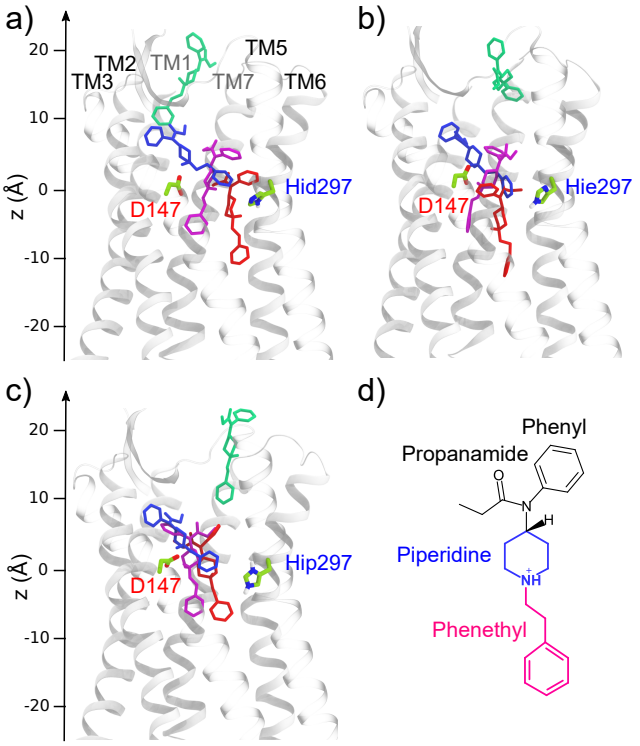

Figure 1. **Fentanyl-mOR dissociation may involve deep insertion of fentanyl. a-c)** Example snapshots from the metadynamics trajectories involving deep insertion of fentanyl in the presence of Hid297 (**a**), Hie297 (**b**), and Hip297 (**c**) . Fentanyl is colored according to the time: blue (beginning), purple (deep pocket), brown (deep pocket at a later time), and green (final). The z axis is shown with the origin at the C_α center-of-mass (COM) of the orthosteric site residues: Y75, Q124, N127, W133, L144, D147, Y148, M151, F152, L232, K233, V236, A240, W293, I296, H297, V300, W318, H319, I322, and Y326 (about the level of D147). **d)** Chemical structure of fentanyl. The phenylpropanamide, piperidine, and phenethyl groups colored black, blue, and magenta, respectively.

the Filizola group.[23] However, surprisingly, we found that 27% Hid, 37% Hie, and 19% Hip trajectories followed the "deep" pathways, in which fentanyl moves below the orthosteric site region (z < -2 Å) before moving up and finally dissociating from the receptor (Fig. 1a-c and Fig. S2). Trajectories following this mechanism show an initial descent of fentanyl's z position (to as low as -10 Å) and concurrent increase in the contact number (to as high as ∼300) before the eventual increase in z and decrease in contact number.

The unbiased (approximate) free energy surfaces (FES') projected onto z and contact number based on the direct and deep pathway trajectories are significantly different (Fig. S3). The FES' based on direct Hid and Hie trajectories show local minimum or minima in the vestibule region, consistent with the simulations of morphine and buprenorphine (the paper did not specify whether Hid297 or Hie297 was used).[23] In contrast, the corresponding FES' based on deep trajectories do not contain local minimum or minima en route to complete dissociation. Importantly, the free energy minimum regions based on the deep Hid and Hie trajectories are deeper than the corresponding direct trajectories by more than 5 kcal/mol, suggesting a potentially significant difference in kinetics. Furthermore, the minimum regions based on the deep trajectories extend below z of 0 Å (about the level of D147), which is in agreement with the WE simulations of fentanyl-mOR dissociation in the presence of Hid297 or Hie297.[16]

Dissociation times for the direct and deep pathways differ by orders of magnitude. Following the work of others,[23,27,28,30] we analyzed the unbiased fentanyl escape times recovered from the individual trajectories using the Poisson distribution (Fig. S4). By fitting to the theoretical cumulative distribution function,[30] the dissociation time τ ($\tau = 1/k_{\text{off}}$) was estimated. Remarkably, the calculated dissociation time for the deep pathways is 2–4 orders of magnitude larger than the direct pathways, consistent with the much deeper free energy minimum. For the deep pathways, the calculated τ values are 27±12 s, 6.1±1 s, and 0.6±0.2 s from Hid, Hie, and Hip trajectories, respectively, whereas the corresponding values for the direct pathways are 8.5±0.8 ms, 12±2 ms and 2±0.2 ms (Table 1 and Fig. S4-S5). The p-values from the two-sample Komologorov-Smirnov test[30] are above 0.05 for accepting the Poisson-fitted τ values, except for the direct trajectories with Hie297 and Hip297, which have smaller p-values indicating that the estimated dissociation times are less accurate.

Table 1. Calculated microscopic fentanyl-mOR dissociation times[a] for the direct and deep pathways with different protonation states of H297$^{6.52}$

H297$^{6.52}$	Direct	Deep
Hid	8.5±0.8 ms	27±12 s
Hie	12±2 ms	6±1 s
Hip	2.0±0.2 ms	0.6±0.2 s

[a] Errors are from the boot-strap analysis. Poisson fitting analysis is given in Fig. S5.

Interestingly, the calculated dissociation time for the deep pathways with Hid297 is within one order of magnitude from the measured residence time of fentanyl ∼4 min (David Strauss and Zhihua Li, submitted to GitHub). It is also consistent with the time range of 0.1 to 10 min for ligand-mOR dissociation.[31] For example, the residence time of carfentanil,[32] which is a fentanyl analog with a methyl ester group at the 4'-axial position, is about 5 min, while buprenorphine's residence time is about 10 min,[33] and naloxone's residence time is about 1 min.[34] Considering the agreement with the experimental timescale and consistency between the approximate FES' and those from the WE simulations, we suggest that the deep insertion pathways may be biologically relevant. Additionally, the calculated dissociation times via the deep pathways are consistent with the measured residence time of 29 s for the binding of a G-protein mimetic Nb39 to fentanyl-bound mOR.[35] Since the full activation of mOR requires the coupling of agonist-bound mOR to a G-protein,[36] this agreement lends further support to the biological relevance of the deep pathways.

Fentanyl interactions with D147$^{3.32}$ and H297$^{6.52}$ in the deep pathways are dependent on the protonation state of H297$^{6.52}$. Given the potential biological relevance of deep insertion, we examined how fentanyl is stabilized there. Our previous work employing the WE and unbiased equilibrium MD simulations suggested that fentanyl can form a hydrogen bond with Hid297, which possibly prolongs the residence time;[16] however, why deep pocket insertion also occurs in the presence of Hie297 and Hip297 is puzzling. To address this question, we calculated the volumetric occupancy map and the unbiased (reweighted) approximate free energy surface (FES) projected onto the distance from piperidine:N to D147:CG ($R_{\text{FEN-D147}}$) and the minimum distance between piperidine:N and H297:ND/NE ($R_{\text{FEN-H297}}$), based on the deep trajectories (Fig. 2). The occupancy map informs the location of fentanyl throughout the dissociation process, and the FES allows examination of fentanyl's interactions with D147 and H297.

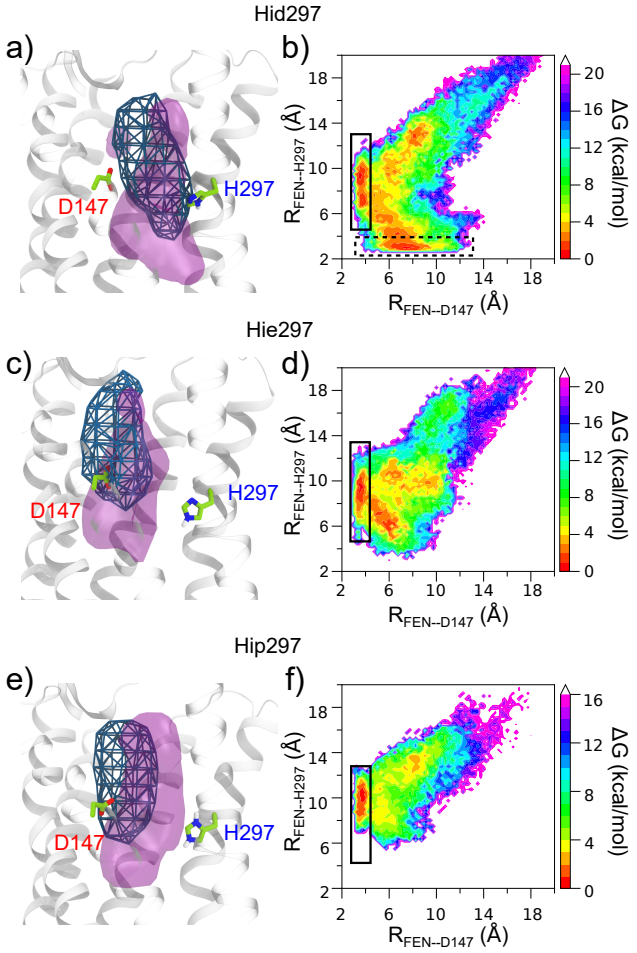

Figure 2. **Fentanyl's location and interactions with D147$^{3.32}$/H297$^{6.52}$ are dependent on the protonation state of H297$^{6.52}$. a,c,e)** Volumetric occupancy map of piperidine (green mesh) and phenethyl (purple) groups obtained from the deep trajectories with Hid297 (**a**), Hie297 (**c**), and Hip297 (**e**). Calculations were performed with the VolMap plugin in VMD[37] (occupancy cutoff of 0.03).The isosurface maps were rendered with VMD.[37] **b,d,f)** The approximate free energy surface (FES) projected onto the distances $R_{\text{FEN-D147}}$ and $R_{\text{FEN-H297}}$ based on the deep trajectories with Hid297 (**b**), Hie (**d**), and Hip (**f**). $R_{\text{FEN-D147}}$ refers to the distance between piperidine:N and D147:CG, and $R_{\text{FEN-H297}}$ refers to the minimum distance between piperidine:N and NE or ND of H297. The FES regions where the D147 salt bridge and the H297 hydrogen bond are formed are highlighted by solid and dashed boxes, respectively. The FES were calculated using a reweighting protocol[38] in PLUMED.[39]

The occupancy maps showed that the fentanyl insertion is deepest in the presence of Hid297 (Fig. 2a,2c,2e), whereby the piperidine and phenethyl groups sample regions near H297 (Fig. 2a). The approximate FES($R_{\text{FEN-D147}}$,$R_{\text{FEN-H297}}$) based on Hid trajectories displays extensive free energy minimum regions; however, two minima are prominent. One minimum is located around (4, 6.5–10.5), indicating that piperidine maintains a salt bridge with D147 with negligible interaction with H297, and another minimum is around (6–10, 2.5), indicating that piperidine forms a hydrogen bond with H297 with negligible interaction with D147 (Fig. 2b). The barrier

between the two minima is very low ($<$ 3 kcal/mol), suggesting that the transition between the two bound states may be facile. Interestingly, while fentanyl maintains the D147 salt bridge (Fig. 2b and S6, black box region), its z varies from -3 to 6 Å. While it maintains the H297 hydrogen bond (Fig. 2b and S7, dashed box region), its z varies from -7 to 1 Å.

Turning to the deep trajectories with Hie297 and Hip297, the occupancy maps show that the piperidine ring does not reach H297, although the phenethyl group samples the regions well below D147 (Fig. 2c and e). Consistently, the FES' display minima corresponding to the piperidine-D147 salt bridge but not the piperidine-H297 hydrogen bond (Fig. 2d and f). Interestingly, the FES of Hie trajectories shows that the minimum region extends down to $R_{FEN\text{-}H297}$ of 4.5 Å, suggesting that piperidine can come into van der Waals contact with H297 (Fig. 2d). In contrast, there is no sampling below $R_{FEN\text{-}H297}$ of 6 Å in Hip trajectories (Fig. S7, right panel), indicating that the piperidine-H297 contact is completely absent. This may be explained by the repulsion between the positively charged piperidine and Hip297, and is consistent with the previous equilibrium MD and CpHMD simulations.[16] Consistent with the Hid deep trajectories, while maintaining the piperidine-D147 salt bridge, fentanyl can sample z positions as low as -5 or -3 Å in presence of Hie297 or Hip297, respectively (Fig. S6, middle and right panels).

Examining the overall FES', we notice that the FES based on the Hip trajectories is significantly shallower (by about 5 kcal/mol) compared to the FES' based on the Hie and Hip trajectories, consistent with the 10–50 times faster dissociation rate of fentanyl in the presence of Hip297 compared to Hie297 or Hid297 (Table 1). Note, when $R_{FEN\text{-}D147}$ and $R_{FEN\text{-}H297}$ are greater than 18 Å, fentanyl is unbound with z above 15 Å (Fig. S6 and S7). Taken together, the above analysis suggests that the deep pathways involve a D147-bound state, and in the presence of Hid297, a H297-bound state is additionally stabilized. Both states can be maintained while fentanyl samples positions well below the D147 level. The latter is readily understood given the lower position of H297 relative to D147;[16] however, it is puzzling as to how a deeply inserted ($z <$ -2 Å) D147-bound state is possible.

Fentanyl-mOR interactions that stabilize the deep-pocket binding. To further understand the deep pocket binding mechanism and the effect of the H297 protonation state, we calculated the increased fractions of contacts between the fentanyl constituent groups and the mOR residues in the deep pocket relative to the direct trajectories (Fig. 3 and Fig. S8). The resulting contact profiles reveal specific fentanyl-mOR interactions that are enriched in the deep pocket binding. In the presence of Hid297, besides the piperidine-H297 hydrogen bond, the most significantly enriched polar contacts are the hydrogen bonds between the propanamide carbonyl and K233 of TM5 or Y148 of TM3, which appear to anchor fentanyl in the deep pocket from the top (Fig. 3a and 3c top panel). The contact profile also shows extensive hydrophobic interactions between all three fentanyl constituent groups and hydrophobic sidechains on TM3/TM5/TM6. The phenyl group attached to propanamide interacts with V236 of TM5 and I296/V300 of TM6, which have similar z positions as $H297^{6.52}$ (Fig. 3c top panel). The piperidine ring interacts with W293, and the phenethyl group forms numerous hydrophobic contacts, with M151/I155/L158 on TM3 and F289/W293 on TM6, all of which are below H297 in the z position (Fig. 3d,e top panels). Note, I155 and F289 belong to the conserved core triad.[7]

A major difference among the fentanyl-mOR contact profiles with Hid/Hie/Hip is in the TM6 interactions (Fig. 3). The piperidine-Hid297 hydrogen bond enables piperidine to interact with W293 and I296 on TM6; such hydrophobic contacts are significantly diminished in the Hie and absent in the Hip deep trajectories. It is worthwhile noticing that the deep insertion in the presence of Hid297 is also facilitated by the phenylpropanamide interactions with I296/V300 on TM6 and phenethyl interaction with F289 (below W293), which are significantly weakened in the Hie and absent in the Hip trajectories. The latter can be explained by the repulsion between the piperidine ring and Hip297. Another major difference between the Hid and Hie/Hip contact profiles is in the D147 interactions. Surprisingly, the piperidine–D147 interaction is enriched in the deep trajectories by more than 25% in the presence of Hie297 or nearly 49% in the presence of Hip297 (Fig. 3d, middle and bottom panels). Trajectory snapshots showed that while maintaining the piperidine-D147 salt bridge, fentanyl can move down, allowing the phenethyl group to form several hydrophobic contacts with deep pocket residues, M151/I155 on TM3 and W293 on TM6 (Fig. 3b). Interestingly, the hydrogen bonds between propanamide and K233 or Y148 are missing in the trajectories with Hip297.

Taken together, the contact analysis suggests that in the presence of Hid297, the formation of the piperidine-H297 hydrogen bond allows the piperidine-D147 salt bridge to be disrupted, enabling fentanyl to descend deeper into mOR. The corresponding switch of the binding mode (from TM3 to TM6) in turn facilitates numerous hydrophobic interactions, particularly with M151/S154/I155 on TM3 and F289/W293 on TM6, which stabilizes the deep-pocket configurations. By contrast, in the presence of Hie297, which is incapable of forming a hydrogen bond with piperidine, while the electrostatic interaction with D147 is maintained, fentanyl can move down due to the hydrophobic interactions with deep pocket residues, such as M151 on TM3 and W293 on TM6, although the number of hydrophobic contacts is smaller compared to those in the Hid trajectories. The contact analysis also suggests that the hydrogen bond interactions of propanamide with K233/Y148 may play a role in assisting fentanyl's deep insertion in the presence of Hid297 or Hie297. Finally, in the presence of Hip297, which electrostatically repels the charged piperidine, the number of hydrophobic contacts particularly with TM6 is significantly reduced. As a result, fentanyl is able to occasionally sample the deep pocket configurations while in the D147 binding mode, but the insertion is shallow, consistent with the fastest dissociation time of the Hip trajectories (Table 1).

CONCLUDING DISCUSSION

In summary, 144 metadynamics simulations were carried out to investigate the mechanism and kinetics of fentanyl-mOR dissociation in the presence of Hid297, Hie297, and Hip297. 73% Hid, 63% Hie, 81% Hip trajectories showed that fentanyl can spontaneously escape from the orthosteric site region, with the corresponding dissociation times of 8.5$\pm$0.8, 12$\pm$2, and 2.0$\pm$0.2 ms. However, in 27% Hid, 37% Hie, and 19% Hip trajectories, fentanyl samples a deep pocket region, up to 10 Å below the orthosteric site (the level of D147), before escaping from the receptor. The calculated dissociation times based on the deep trajectories are 27$\pm$12 s, 6$\pm$1 s, and 0.6$\pm$0.2 s in the presence of Hid297, Hie297, and Hip297, respectively. The former dissociation time is within one or-

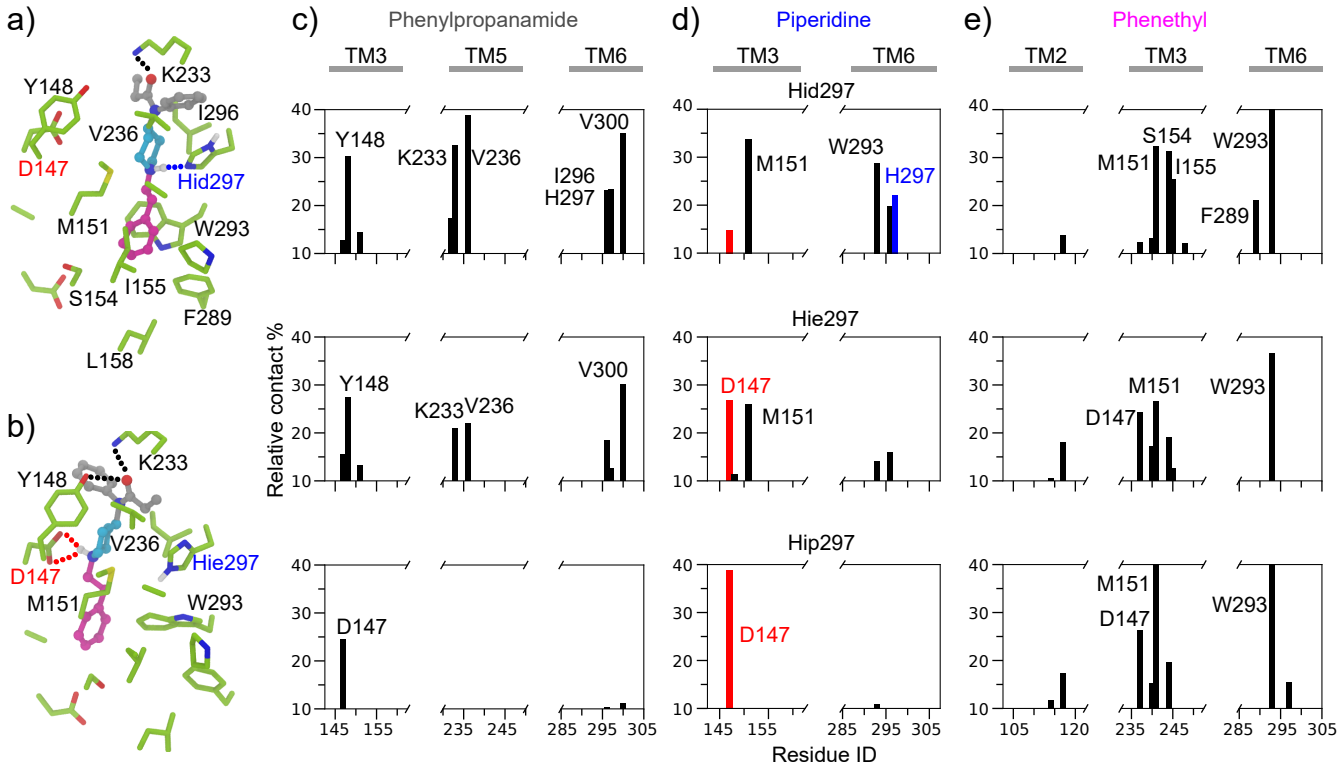

Figure 3. **Deep pocket binding is stabilized by different fentanyl-mOR interactions depending on the protonation state of H297$^{6.52}$. a,b)** Representative snapshots showing fentanyl in the deep pocket stabilized by the piperidine-Hid297 hydrogen bond (**a**) or the piperidine-D147 salt bridge (**b**). The phenylpropanamide, piperidine, and phenethyl groups are colored grey, blue, and magenta, respectively. Residues contacting fentanyl are shown in green and labeled. **c,d,e)** Relative fractions of contacts between mOR residues and the phenylpropanamide (**c**), piperidine (**d**), or phenethyl (**e**) group calculated from the deep vs. direct trajectories in the presence of Hid297 (top), Hie297 (middle), or Hip297 (bottom). Only positive relative contact fractions $\geq$10% are displayed. Residues with relative contact fractions $\geq$20% are labeled and displayed in panels a) and b). The contacts are defined using a 4.5-Å distance cutoff between heavy atoms.

der of magnitude from the recently measured value of $\sim$4 min (Strauss and Li, submitted to GitHub), suggesting that the observed deep insertion mechanism may be biologically relevant.

Analysis showed that deep insertion is compatible with both D147- and H297-binding modes. In the presence of Hid297, the formation of the piperidine-Hid297 hydrogen bond enables the deep insertion to be stabilized by extensive hydrophobic interactions, particularly with TM6 residues. In the presence of Hie297 or Hip297, fentanyl can sample the deep pocket via hydrophobic contacts, while maintaining the electrostatic interaction with D147. In the presence of Hip297, the electrostatic repulsion with the piperidine prohibits or weakens the contacts with TM6 residues, which may explain why the insertion is much shallower and dissociation time is decreased by 1 or 2 orders of magnitude compared to the Hie or Hid trajectories, respectively. Interestingly, all residues that are involved in the deep pocket contacts are conserved. Given the central role that TM6 plays in the mOR activation, the hydrophobic interactions with TM6 residues such as W293, F289, and V300 may be functionally relevant. Future studies aimed at the conformational transitions of mOR may provide further insights.

The dissociation mechanism of fentanyl uncovered by our study differs significantly from that of morphine and buprenorphine, which were found to dissociate directly from the orthosteric site region in a recent metadynamics study by the Filizola group (15 trajectories, H297$^{6.52}$ protonation state unclear).[23] This is however not surprising, as fentanyl differs from morphine in many aspects. The elongated shape of fentanyl may allow it to insert deep into mOR, which may not be possible with bulkier ligands such as morphine and analogs. Fentanyl's deep insertion is also consistent with a previous study, which found that acetylcholine (a small elongated molecule) can diffuse into a deep pocket of M3 and M4 muscarinic acetylcholine receptors.[20] Preclinical pharmacology studies demonstrated that fentanyl displays a bias for β-arrestin relative to G-protein signaling, which is in contrast to morphine that displays a modest bias for G protein signaling.[4,40] The significant pharmacological difference has been speculated as a result of the different mechanism of binding and activation.[5] The present metadynamics data adds to the evidence in support of this hypothesis.

A main caveat of the present work is the use of a modeled, albeit equilibrated structure of the mOR-fentanyl complex to initiate the dissociation simulations. Consequently, the direct pathways that have 3-5 orders of magnitude faster rates than the experimental measurements may be an artifact due to the starting structure not residing in a global free energy minimum. This consideration is supported by our contact analysis which showed that the D147 binding mode is strengthened in the deep trajectories, and our recent long-time-scale unbiased simulation data which suggests that fentanyl's COM position can sample below the level of D147 (Ref.[16] and Fig. S9). Additional caveats include the neglect of the potential conformational deactivation of mOR induced by fentanyl dissociation, which may somewhat affect the calculated rates. Due to the biased nature of metadynamics, the kinetic cal-

culations as well as the fentanyl-mOR interactions and unbiased free energies have limited accuracy. Nonetheless, the aforementioned caveats are not expected to alter our conclusions regarding the mechanism of deep pocket insertion and the profound effect of H297$^{6.52}$ protonation state. To test the generality of the deep pocket binding mechanism and to further explore the role of H297$^{6.52}$, a systematic study of fentanyl and morphine analogs is underway. Our work provides a computational protocol that can be used to predict the dissociation rates of opioids to assist the regulatory evaluation of strategies for drug overdose reversal. The profound role of histidine protonation state discovered here may shift the paradigm in computational studies of ligand-receptor kinetics which is gaining increased attention.

Methods and Protocols. The protein and lipids (POPC (1-palmitoyl-2-oleoyl-glycero-3-phosphocholine) and cholesterol) were represented by the CHARMM c36m protein[41,42] and c36 lipid[43] force fields, respectively. Water was represented by the CHARMM-style TIP3P force field.[44] The parameters for fentanyl were obtained using the ParamChem CGENFF server.[45] Using NAMD 2.13,[46] We first carried out 100-ns MD simulations of the the membrane-embedded apo mOR based on the BU72-mOR complex crystal structure (PDB:5C1M)[7] at 1 atm and 310 K. The protonation states were determined by the membrane-enabled hybrid-solvent continuous constant pH molecular dynamics (CpHMD) method with pH replica exchange[47,48] in CHARMM.[44] A fentanyl-bound mOR model was prepared by superimposing a top fentanyl binding pose obtained from a previous docking study[13] onto the equilibrated structure of membrane-embedded apo mOR. The resulting model of the fentanyl-mOR complex was then relaxed in 65-ns NPT simulations at 1 atm and 310 K and used as a starting structure for the equilibration simulation before metadynamics.

The well-tempered metadynamics simulations[25] were performed for the membrane-embedded fentanyl-mOR complex using the Collective Variables (ColVars) module[49] in NAMD 2.13.[46] 48 independent metadynamics runs were performed with each of the 3 protonation states of H297$^{6.52}$ (Hid, Hie, and Hip), amounting to a total of 144 simulations with an aggregate time of $\sim$4 μs. The center-of-mass z position of fentanyl relative to that of the orthosteric site Cα atoms (defined in Fig. 1) and the fentanyl-mOR contact number (CN) were used as the collective variables.

$$\mathrm{CN} = \frac{1-(d/4.5)^8}{1-(d/4.5)^{16}}. \quad (1)$$

A Gaussian bias potential was deposited every 10 ps, as in the previous metadynamics studies of inhibitor-kinase unbinding kinetics.[27,28] Note, our test simulations with 20 or 30 ps deposition time did not result in significant differences in the calculated dissociation times.

Supporting Information Available. Methods and Protocols, and additional figures are provided in Supporting Information.

Acknowledgement. P. M. and Q.N.V. are supported by ORISE fellowships through an interagency agreement between the Department of Energy and FDA. Financial support from the National Institutes of Health (R01GM098818) to J.S. is acknowledged. We thank Pratyush Tiwary for the helpful discussion of metadynamics simulations. We also thank David G. Strauss and Zhihua Li for sharing with us their kinetic measurement data of fentanyl. Disclaimer: the findings and conclusions in this manuscript have not been formally disseminated by the FDA and should not be construed to represent any agency determination or policy.

References

(1) Armenian, P.; Vo, K. T.; Barr-Walker, J.; Lynch, K. L. Fentanyl, Fentanyl Analogs and Novel Synthetic Opioids: A Comprehensive Review. *Neuropharmacol.* **2018**, *134*, 121–132.
(2) Throckmorton, D. C.; Gottlieb, S.; Woodcock, J. The FDA and the Next Wave of Drug Abuse — Proactive Pharmacovigilance. *N. Engl. J. Med.* **2018**, *379*, 205–207.
(3) Coronavirus Disease 2019. https://www.cdc.gov/media/releases/2020/p1218-overdose-deaths-covid-19.html, 2020.
(4) Comer, S. D.; Cahill, C. M. Fentanyl: Receptor Pharmacology, Abuse Potential, and Implications for Treatment. *Neurosci. Biobehav. Rev.* **2019**, *106*, 49–57.
(5) Burns, S. M.; Cunningham, C. W.; Mercer, S. L. DARK Classics in Chemical Neuroscience: Fentanyl. *ACS Chem. Neurosci.* **2018**, *9*, 2428–2437.
(6) Darcq, E.; Kieffer, B. L. Opioid Receptors: Drivers to Addiction? *Nat. Rev. Neurosci.* **2018**, *19*, 499–514.
(7) Huang, W. et al. Structural Insights into μ-Opioid Receptor Activation. *Nature* **2015**, *524*, 315–321.
(8) Manglik, A.; Kruse, A. C.; Kobilka, T. S.; Thian, F. S.; Mathiesen, J. M.; Sunahara, R. K.; Pardo, L.; Weis, W. I.; Kobilka, B. K.; Granier, S. Crystal Structure of the M-Opioid Receptor Bound to a Morphinan Antagonist. *Nature* **2012**, *485*, 321–326.
(9) Koehl, A. et al. Structure of the μ-Opioid Receptor-Gi Protein Complex. *Nature* **2018**, *558*, 547–552.
(10) Katritch, V.; Cherezov, V.; Stevens, R. C. Structure-Function of the G Protein–Coupled Receptor Superfamily. *Annu. Rev. Pharmacol. Toxicol.* **2013**, *53*, 531–556.
(11) Ballesteros, J. A.; Weinstein, H. In *Methods in Neurosciences*; Sealfon, S. C., Ed.; Receptor Molecular Biology; Academic Press, 1995; Vol. 25; pp 366–428.
(12) Surrat, C. K.; Johnson, P. S.; Moriwaki, A.; Seidleck, B. K.; Blaschak, C. J.; Wang, J. B.; Uhl, G. R. Charged Transmembrane Domain Amino Acids Are Critical for Agonist Recognition And Intrinsic Activity. *J. Biol. Chem.* **1994**, *269*, 20548–20553.
(13) Ellis, C. R.; Kruhlak, N. L.; Kim, M. T.; Hawkins, E. G.; Stavitskaya, L. Predicting Opioid Receptor Binding Affinity of Pharmacologically Unclassified Designer Substances Using Molecular Docking. *PLoS One* **2018**, *13*, e0197734.
(14) Lipiński, P. F. J.; Jarończyk, M.; Dobrowolski, J. C.; Sadlej, J. Molecular Dynamics of Fentanyl Bound to μ-Opioid Receptor. *J. Mol. Model.* **2019**, *25*, 144.
(15) Lipiński, P. F. J.; Kosson, P.; Matalińska, J.; Roszkowski, P.; Czarnocki, Z.; Jarończyk, M.; Misicka, A.; Dobrowolski, J. C.; Sadlej, J. Fentanyl Family at the Mu-Opioid Receptor: Uniform Assessment of Binding and Computational Analysis. *Molecules* **2019**, *24*, 740.
(16) Vo, Q. N.; Mahinthichaichan, P.; Shen, J.; Ellis, C. R. How μ-Opioid Receptor Recognizes Fentanyl. *Nat. Commun.* **2021**, *xx*, xx.
(17) Mansour, A.; Taylor, L. P.; Fine, J. L.; Thompson, R. C.; Hoversten, M. T.; Mosberg, H. I.; Watson, S. J.; Akil, H. Key Residues Defining the μ-Opioid Receptor Binding Pocket: A Site-Directed Mutagenesis Study. *J. Neurochem.* **1997**, *68*, 344–353.
(18) Meyer, J.; Del Vecchio, G.; Seitz, V.; Massaly, N.; Stein, C. Modulation of M-opioid Receptor Activation by Acidic pH Is Dependent on Ligand Structure and an Ionizable Amino Acid Residue. *Br. J. Pharmacol.* **2019**, *176*, 4510–4520.
(19) Pan, A. C.; Borhani, D. W.; Dror, R. O.; Shaw, D. E. Molecular Determinants of Drug–Receptor Binding Kinetics. *Drug Discovery Today* **2013**, *18*, 667–673.
(20) Chan, H. C. S.; Wang, J.; Palczewski, K.; Filipek, S.; Vogel, H.; Liu, Z.-J.; Yuan, S. Exploring a New Ligand Binding Site of G Protein-Coupled Receptors. *Chem. Sci.* **2018**, *9*, 6480–6489.
(21) Alfonso-Prieto, M.; Navarini, L.; Carloni, P. Understanding Ligand Binding to G-Protein Coupled Receptors Using Multiscale Simulations. *Frontiers in Molecular Biosciences* **2019**, *6*, 29.
(22) Potterton, A.; Husseini, F. S.; Southey, M. W. Y.; Bodkin, M. J.; Heifetz, A.; Coveney, P. V.; Townsend-Nicholson, A. Ensemble-Based Steered Molecular Dynamics Predicts Relative Residence Time of A $_{2A}$ Receptor Binders. *J. Chem. Theory Comput.* **2019**, *15*, 3316–3330.
(23) Lamim Ribeiro, J. M.; Provasi, D.; Filizola, M. A Combination of Machine Learning and Infrequent Metadynamics to Efficiently Predict Kinetic Rates, Transition States, and Molecular Determinants of Drug Dissociation from G Protein-Coupled Receptors. *J. Chem. Phys.* **2020**, *153*, 124105.
(24) Laio, A.; Parrinello, M. Escaping Free-Energy Minima. *Proc. Natl. Acad. Sci.* **2002**, *99*, 12562–12566.
(25) Barducci, A.; Bussi, G.; Parrinello, M. Well-Tempered Metadynamics: A Smoothly Converging and Tunable Free-Energy Method. *Phys. Rev. Lett.* **2008**, *100*, 020603.

(26) Callegari, D.; Lodola, A.; Pala, D.; Rivara, S.; Mor, M.; Rizzi, A.; Capelli, A. M. Metadynamics Simulations Distinguish Short- and Long-Residence-Time Inhibitors of Cyclin-Dependent Kinase 8. *J. Chem. Inf. Model.* **2017**, *57*, 159–169.
(27) Casasnovas, R.; Limongelli, V.; Tiwary, P.; Carloni, P.; Parrinello, M. Unbinding Kinetics of a P38 MAP Kinase Type II Inhibitor from Metadynamics Simulations. *J. Am. Chem. Soc.* **2017**, *139*, 4780–4788.
(28) Tiwary, P.; Mondal, J.; Berne, B. J. How and When Does an Anticancer Drug Leave Its Binding Site? *Sci. Adv.* **2017**, *3*, e1700014.
(29) Capelli, R.; Lyu, W.; Bolnykh, V.; Meloni, S.; Olsen, J. M. H.; Rothlisberger, U.; Parrinello, M.; Carloni, P. Accuracy of Molecular Simulation-Based Predictions of k_{off} Values: A Metadynamics Study. *J. Phys. Chem. Lett.* **2020**, *11*, 6373–6381.
(30) Salvalaglio, M.; Tiwary, P.; Parrinello, M. Assessing the Reliability of the Dynamics Reconstructed from Metadynamics. *J. Chem. Theory Comput.* **2014**, *10*, 1420–1425.
(31) Strasser, A.; Wittmann, H.-J.; Seifert, R. Binding Kinetics and Pathways of Ligands to GPCRs. *Trends Pharmacol. Sci.* **2017**, *38*, 717–732.
(32) Titeler, M.; Lyon, R. A.; Kuhar, M. J.; Frost, J. F.; Dannals, R. F.; Leonhardt, S.; Price, D. L.; Struble, R. G. Opiate Receptors Are Selectively Labelled by [3H]Carfentanil in Human and Rat Brain. *Eur. J. Pharmacol.* **1989**, *167*, 221–228.
(33) Pedersen, M. F.; Wróbel, T. M.; Märcher-Rørsted, E.; Pedersen, D. S.; Møller, T. C.; Gabriele, F.; Pedersen, H.; Matosiuk, D.; Foster, S. R.; Bouvier, M.; Bräuner-Osborne, H. Biased Agonism of Clinically Approved μ-Opioid Receptor Agonists and TRV130 Is Not Controlled by Binding and Signaling Kinetics. *Neuropharmacol.* **2020**, *166*, 107718.
(34) Cassel, J. A.; Daubert, J. D.; DeHaven, R. N. [3H]Alvimopan Binding to the μ Opioid Receptor: Comparative Binding Kinetics of Opioid Antagonists. *Eur. J. Pharmacol.* **2005**, *520*, 29–36.
(35) Livingston, K. E.; Mahoney, J. P.; Manglik, A.; Sunahara, R. K.; Traynor, J. R. Measuring Ligand Efficacy at the Mu-Opioid Receptor Using a Conformational Biosensor. *eLife* **2018**, *7*, e32499.
(36) Sounier, R.; Mas, C.; Steyaert, J.; Laeremans, T.; Manglik, A.; Huang, W.; Kobilka, B. K.; Déméné, H.; Granier, S. Propagation of Conformational Changes during μ-Opioid Receptor Activation. *Nature* **2015**, *524*, 375–378.
(37) Humphrey, W.; Dalke, A.; Schulten, K. VMD: Visual Molecular Dynamics. *J. Mol. Graph.* **1996**, *14*, 33–38.
(38) Tiwary, P.; Parrinello, M. A Time-Independent Free Energy Estimator for Metadynamics. *J. Phys. Chem. B* **2015**, *119*, 736–742.
(39) Tribello, G. A.; Bonomi, M.; Branduardi, D.; Camilloni, C.; Bussi, G. PLUMED 2: New Feathers for an Old Bird. *Comput. Phys. Commun.* **2014**, *185*, 604–613.
(40) Schmid, C. L.; Kennedy, N. M.; Ross, N. C.; Lovell, K. M.; Yue, Z.; Morgenweck, J.; Cameron, M. D.; Bannister, T. D.; Bohn, L. M. Bias Factor and Therapeutic Window Correlate to Predict Safer Opioid Analgesics. *Cell* **2017**, *171*, 1165–1175.e13.
(41) Best, R. B.; Zhu, X.; Shim, J.; Lopes, P. E. M.; Mittal, J.; Feig, M.; MacKerell, A. D. Optimization of the Additive CHARMM All-Atom Protein Force Field Targeting Improved Sampling of the Backbone ϕ, ψ and Side-Chain χ_1 and χ_2 Dihedral Angles. *J. Chem. Theory Comput.* **2012**, *8*, 3257–3273.
(42) Huang, J.; Rauscher, S.; Nawrocki, G.; Ran, T.; Feig, M.; de Groot, B. L.; Grubmüller, H.; MacKerell, A. D. CHARMM36m: An Improved Force Field for Folded and Intrinsically Disordered Proteins. *Nat. Methods* **2017**, *14*, 71–73.
(43) Klauda, J. B.; Venable, R. M.; Freites, J. A.; O'Connor, J. W.; Tobias, D. J.; Mondragon-Ramirez, C.; Vorobyov, I.; MacKerell, A. D.; Pastor, R. W. Update of the CHARMM All-Atom Additive Force Field for Lipids: Validation on Six Lipid Types. *J. Phys. Chem. B* **2010**, *114*, 7830–7843.
(44) Brooks, B. R. et al. CHARMM: The Biomolecular Simulation Program. *J. Comput. Chem.* **2009**, *30*, 1545–1614.
(45) Vanommeslaeghe, K.; Raman, E. P.; MacKerell, A. D. Automation of the CHARMM General Force Field (CGenFF) II: Assignment of Bonded Parameters and Partial Atomic Charges. *J. Chem. Inf. Model.* **2012**, *52*, 3155–3168.
(46) Phillips, J. C.; Braun, R.; Wang, W.; Gumbart, J.; Tajkhorshid, E.; Villa, E.; Chipot, C.; Skeel, R. D.; Kalé, L.; Schulten, K. Scalable Molecular Dynamics with NAMD. *J. Comput. Chem.* **2005**, *26*, 1781–1802.
(47) Wallace, J. A.; Shen, J. K. Continuous Constant pH Molecular Dynamics in Explicit Solvent with pH-Based Replica Exchange. *J. Chem. Theory Comput.* **2011**, *7*, 2617–2629.
(48) Chen, W.; Huang, Y.; Shen, J. Conformational Activation of a Transmembrane Proton Channel from Constant pH Molecular Dynamics. *J. Phys. Chem. Lett.* **2016**, *7*, 3961–3966.
(49) Fiorin, G.; Klein, M. L.; Hénin, J. Using Collective Variables to Drive Molecular Dynamics Simulations. *Mol. Phys.* **2013**, *111*, 3345–3362.
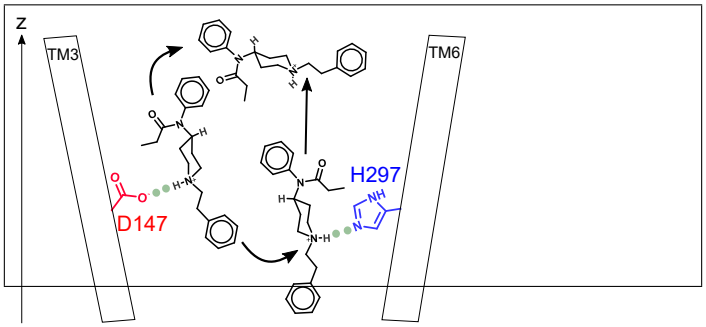
Graphical TOC Entry